Reviews

Structural Predictions in the ABO_3 Phase Diagram

Daniel M. Giaquinta and Hans-Conrad zur Loye*

Department of Chemistry, Massachusetts Institute of Technology, Cambridge, Massachusetts 02139

Received October 26, 1993®

Several approaches for predicting the structures of ABO_3 compounds are discussed and contrasted. The basic principles behind structure–composition predictions are reviewed, and a new approach for structural prediction that relies on the combination of ionic radii and bond ionicities is introduced. The major ABO_3 structures are described, and the criteria that govern their formation for different elements are examined. Two structural phase diagrams for ABO_3 compounds are analyzed and a new transition metal structure type, $InMO_3$ (M = Mn, Fe), is explained within the context of the ABO_3 structural phase diagrams. Several compounds with the $InMO_3$ structure are predicted.

Introduction

The rational design of advanced materials assumes an understanding of the correlation between basic crystal chemistry and simple structure–property relationships. Implicit in such a relationship is an understanding of the connection between chemical composition and crystal structure in solid-state materials. Properties such as electronegativity, radii, valence electron count, and principal quantum number can help establish a link between composition, structure, and properties for different classes of materials. Establishing such a link, however, is particularly difficut due to the large number of parameters which affect structures including the charge and coordination preferences of metals, the existence of energetically close-lying structure types, and synthetic parameters, e.g., pressure and temperature. The use of high-pressure or low-temperature synthesis complicates the problem through the introduction of kinetic considerations and the possibility of metastable phases. Numerous attempts have been made to correlate structural stability with chemical or physical variables derived from atomic properties of the constituent elements; however, for different classes of materials, different atomic properties must be used to achieve good correlation.[1]

Structural prediction based on easily obtainable parameters for compounds with novel compositions, consequently, remains an important problem in the area of solid-state chemistry. Structure types of new compositions often may be predicted accurately if the synthesis involves a cationic, isovalent substitution in a known structure. Structural prediction for new combinations of both cations and anions, however, remains troublesome. The problem of structural prediction has been addressed by many researchers,[2-17] who have used Coulombic, geometric, and quantum mechanical parameters in attempts to model known structures accurately and to predict the structures of unprepared compounds. Although certain approaches, such as the use of pseudopotential radii and electronegativity described by Villars,[15] have been successful for intermetallics, a different approach is necessary to interpret the complex interactions that effect the structure of transition metal oxides.

The problem of structural prediction is particularly acute for transition-metal oxides because of the degree of ionic-covalent bonding present and the competing interactions that this type of bonding generates. These interactions include lattice energies, a Coulombic contribution;[18] crystal-field stabilization energies, an electronic contribution;[19] and geometric packing effects, a steric contribution.[20] Because of this complexity, competing structures may have energy differences on the order of only 0.1 eV/atom,[21] and, therefore, predicting the structure type for a certain elemental composition is difficult. Consequently, while accurate predictive methods exist for

* To whom all correspondence should be addressed.

® Abstract published in *Advance ACS Abstracts*, March 15, 1994.

(1) Kiselyova, N. N. *MRS Bull.* **1993**, *18*, 40.
(2) Adams, D. M. *Inorganic Solids*; John Wiley & Sons: London, 1974; Chapter 5, p 105.
(3) Brewer, L. *Science* **1968**, *161*, 115.
(4) Goldschmidt, V. M. *Mat.-Naturv. Kl.* **1926**, *2*, 117.
(5) Gorter, E. W. *J. Solid State Chem.* **1970**, *1*, 279.
(6) Hume-Rothery, W. *Electrons, Atoms, Metals and Alloys*, 3rd ed.; Dover: New York, 1963.
(7) Laves, F. *Theory of Alloy Phases*; American Society for Metals: Cleveland, 1955; p 124.
(8) Mooser, E.; Pearson, W. B. *Acta Crystallogr.* **1959**, *12*, 1015.
(9) Phillips, J. C.; Van Vechten, J. A. *Phys. Rev. B* **1970**, *2*, 2147.
(10) Phillips, J. C. *Rev. Mod. Phys.* **1970**, *42*, 317.
(11) Roth, R. S. *J. Res. NBS* **1957**, *58*, 75.
(12) Van Vechten, J. A. *Phys. Rev.* **1969**, *187*, 1007.
(13) Van Vechten, J. A.; Phillips, J. C. *Phys. Rev. B* **1970**, *2*, 2160.
(14) Villars, P. *J. Less Common-Met.* **1986**, *119*, 175.
(15) Villars, P.; Hulliger, F. *J. Less-Common Met.* **1987**, *132*, 289.
(16) Villars, P.; Mathis, K.; Hulliger, F. In *Structures of Binary Compounds*; de Boer, F., Pettifor, D., Eds.; North-Holland: Amsterdam, 1989; Vol. 2, p 1.
(17) Villars, P.; Phillips, J. C.; Rabe, K. M.; Brown, I. D. *Ferroelectrics* **1992**, *130*, 129.
(18) Greenwood, N. N. *Ionic Crystals, Lattice Defects, and Nonstoichiometry*; Butterworth: London, 1968.
(19) Orgel, L. E. *Transition-Metal Chemistry: Ligand Field Theory*; Methuen: London, 1963.
(20) Wells, A. F. *Structural Inorganic Chemistry*, 5th ed.; Clarendon Press: Oxford, 1984.
(21) Villars, P. *J. Less-Common Met.* **1983**, *92*, 215.

0897-4756/94/2806-0365$04.50/0

organic compounds, inorganic molecular complexes,[19] metals, and alloys,[3,6,16] the many competing interactions that contribute to the final structure of an ionic–covalent crystal lattice leaves the area of ionic compounds without an equally reliable technique. Thus, in the analysis of transition metal oxides, as discussed below, there is difficulty both in (a) the accurate prediction of structures and (b) the rationalization of structures after they are determined.

Although several predictive methods exist for ionic compounds, each has noticeable shortcomings. In this review, we describe past approaches that have been used for predicting composition–structure relationships for ABO_3 compounds, and we introduce a new approach for structural prediction that relies on the combination of ionic radii and bond ionicities. Our approach, similar to an earlier method described by Mooser and Pearson,[8] uses a combination of ionic radii and valence-specific electronegativity[22] to exploit the subtle differences between the oxidation states of a given element in the structural segregation of ABO_3 compounds. The use of oxidation state-specific electronegativities and ionic radii is crucial since many examples exist where a simple metal oxide crystallizes in unrelated structures for each oxidation state, e.g., the corundum structure of Ti_2O_3 vs the rutile structure of TiO_2.

Using the combination of ionic radii and bond ionicities, the ABO_3 structural phase diagram is discussed, particularly as it applies to two new indium transition-metal oxides, $InMnO_3$ and $InFeO_3$, that have recently been reported.[23,24] The use of this technique, in conjunction with previously developed methods, yields more insight into the ABO_3 structural phase diagram than with any method used alone.

Background

In the past, relationships between structure and composition have been based primarily on close-packing or nondirectional ionic bonding, using space filling, symmetry, and connectivity arguments.[7] Structural arguments based on the simple theory of Coulombic interactions inevitably led to radius-ratio rules. Radius-ratio rules, in spite of some shortcomings, have enjoyed much popularity[2] due to the ease with which they provide structural predictions from readily available factors. This approach was initially limited to simple ionic compounds, and, consequently, the directionality of bonding was introduced to establish improved relationships between structure and elemental composition. Early examples include the Hume-Rothery rules,[6] the Brewer–Engel theory,[3] and more recently, the quantum structural diagrams by Villars which systematize the relationship between composition and structure for intermetallic compounds successfully.[15]

To generalize directional bonding arguments effectively, the problem of identifying parameters that accurately represent the character and directionality of bonding becomes acute. One obvious parameter giving information regarding the character of a bond is electronegativity. The larger the difference in electronegativity ($\Delta\chi$) between two bonded atoms, the greater the ionicity of the bond, while a smaller electronegativity difference indicates greater covalency or metallic character. A second parameter providing a direct correlation with the directionality of a bond is the principle quantum number, n. As n increases, the atomic orbitals involved in bond formation become more diffuse, and, consequently, the bonds lose their directional character. The concept of directionality was utilized by Mooser and Pearson to predict structures for A_aB_b semiconductors.[8] Using the average quantum number of A and B, $\bar{n}$, Mooser and Pearson applied the bond directionality principle and demonstrated that different A_bB_b structures fall into distinct $\bar{n}$ vs $\Delta\chi$ regions. This approach was successful for binary main-group and binary transition-metal compounds.

A more recent refinement to this approach introduced by Phillips and Van Vechten[9,10,12,13] uses a spectroscopically defined ionicity for chemical bonds in A^NB^{8-N} compounds with great accuracy. The need for spectroscopic measurements, however, decreases the ability to use this method in a predictive fashion.

Another approach for predicting intermetallic compounds was taken by Villars,[14–17,21,25,26] who used three-dimensional structural stability diagrams to correlate structures with atomic properties. Villars plotted pseudopotential radius sums vs an average valence electron count vs differences in the Martynov–Batsanov[22] electronegativities. This approach works well for binary, ternary, and quaternary intermetallic compounds and achieves good separation between different structures. Pseudopotential radii, however, are atomic parameters highly correlated with atomic number. Pseudopotential trends in radius ratios differ significantly from trends for ionic radii, and differences due to oxidation states are entirely absent. Pseudopotential radii, thus, are not generally applicable for use in describing ionic materials.

While the above methods have been successful primarily for intermetallic materials, the approach must be modified when analyzing compounds such as oxides. Different properties are indicative of the basic characteristics of an ionic vs an intermetallic structure. For ternary ionic structures, the different properties of the A and B cations should be treated separately and not averaged. Particularly, cations and anions must be treated separately. Compounds containing structural regions with differing ionicities are also a consideration, particularly compounds with low dimensional structural units that contain noninterpenetrating slabs of A–O and B–O, such as $InMnO_3$ and $InFeO_3$.[23,24] Roth, who investigated the structure of $A^{3+}B^{3+}O_3$ compounds,[11,27–29] used the concept of radius ratios to deal with both cations independently and plotted the radius of A vs the radius of B. This approach, shown in Figure 1, separates the main structure types: A–M_2O_3 and B–M_2O_3, perovskite, bixbyite (C–M_2O_3), and corundum (α-Al_2O_3).[29–39] Although materials with the ilmenite

(22) Martynov, A. I.; Batsanov, S. S. *Russ. J. Inorg. Chem.* **1980**, *25*, 1737.
(23) Giaquinta, D. M.; zur Loye, H.-C. *J. Am. Chem. Soc.* **1993**, *114*, 10952.
(24) Giaquinta, D. M.; Davis, W. M.; zur Loye, H.-C. *Acta Crystallogr.* **1994**, *C50*, 5–7.
(25) Villars, P. *J. Less Common-Met.* **1984**, *102*, 199.
(26) Villars, P. *J. Less-Common Met.* **1984**, *99*, 33.
(27) Roth, R. S.; Schneider, S. J. *J. Res. NBS* **1960**, *64A*, 309.
(28) Schneider, S. J.; Roth, R. S. *J. Res. NBS* **1960**, *64A*, 317.
(29) Schneider, S. J.; Roth, R. S.; Waring, J. L. *J. Res. NBS* **1961**, *65A*, 345.
(30) Galasso, F. S. *Structure, Properties and Preparation of Perovskite Type Compounds*; Pergamon Press: Oxford, 1969.
(31) Goodenough, J. B.; Longo, J. M. *Landolt-Bornstein Tabellen, New Series, III*; 1970; Vol. 4a.
(32) Goodenough, J. B. *Prog. Solid State Chem.* **1971**, *5*, 145.

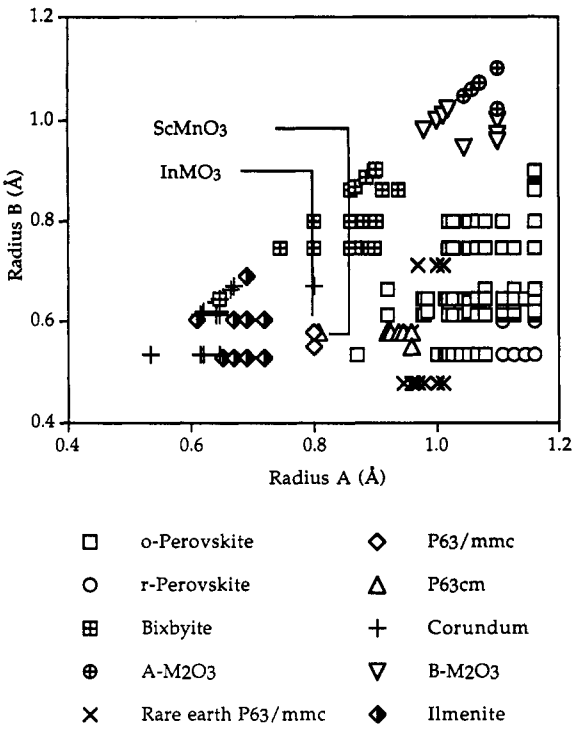

Figure 1. Ionic radii A vs ionic radii B for compounds of the common ABO_3 structure types (after Roth[11]). Included compounds are listed in Table 1.

structure are generally $A^{2+}B^{4+}O_3$, this structure type has been included in Figure 1 for completeness. Roth's method has proven useful for gross structural separations; however, the regions bordering different structural types are not well defined, particularly in the area of the corundum, ilmenite and bixbyite structures, i.e., when both the A and B cations are fairly small.

Other methods, including those of Villars,[17] have been applied to structure–property problems of ternary and quaternary ionic compounds; however, the Villars method requires averaging the atomic properties of the metals present. In the case of a compound with low-dimensional structural units, averaging would, by necessity, obscure the differences between metals that may be responsible for the formation of both a layered structure and low-dimensional properties. By treatment of each metal separately, the differences between metals can be directly observed using a combination of bond ionicities and ionic radii. In the following sections, ideas concerning structural stability diagrams of ABO_3 materials are presented. The common ABO_3 structure types are described and compared with that of $InFeO_3$ and $InMnO_3$, an unusual hexagonal ABO_3 structure type that is unexpected according to known structure–composition diagrams. Using a combination of radius ratios and bond ionicities the existence of the $InMO_3$ structure type is discussed, within the context of the common ABO_3 structure types, perovskite, corundum, ilmenite, and bixbyite (C–M_2O_3); arguments for the

(33) Smyth, D. M. *Annu. Rev. Mater. Sci.* **1985**, *15*, 329.
(34) Rao, C. N. R. *Annu. Rev. Phys. Chem.* **1989**, *40*, 291.
(35) Yakel, H. L., Jr. *Acta Crystallogr.* **1955**, *8*, 394.
(36) Mouron, P.; Choisnet, J.; Abs-Wurmach, I. *Eur. J. Solid State Inorg. Chem.* **1989**, *26*, 35.
(37) Norrestam, R. *Acta Chem. Scand.* **1967**, *21*, 2871.
(38) Newnham, R. E.; Fang, J. H.; Santoro, R. P. *Acta Crystallogr.* **1964**, *17*, 240.
(39) Chamberland, B. L.; Sleight, A. W.; Weiher, J. R. *J. Solid State Chem.* **1970**, *1*, 512.

Table 1. Examples of the Common Structures in the ABO_3 Phase Diagram

o-perovskite	ref	o-perovskite	ref	o-perovskite	ref
$PrScO_3$	29	$PrCrO_3$	29	$EuScO_3$	29
$NdScO_3$	29	$NdCrO_3$	29	$DyScO_3$	29
$GdScO_3$	29	$LaGaO_3$	29	$LaErO_3$	27
$ScAlO_3$	58	$PrGaO_3$	29	$LaTmO_3$	27
$YGaO_3$	56	$NdGaO_3$	29	$LaYbO_3$	27
$InRhO_3$	59	$PrVO_3$	52	$LaLuO_3$	27
$LaMnO_3$	66	$YScO_3$	52	$LaRhO_3$	74
$YAlO_3$	51	$SmAlO_3$	48	$NdRhO_3$	75
$EuAlO_3$	48	$SmCrO_3$	29	$LaYO_3$	11
$GdAlO_3$	48	$LaInO_3$	29	$DyInO_3$	59
$TmAlO_3$	29	$NdInO_3$	29	$TlFeO_3$	59
$DyAlO_3$	29	$SmInO_3$	29	$TlCrO_3$	59
$HoAlO_3$	29	$EuCrO_3$	29	$GdInO_3$	59
$ErAlO_3$	29	$GdCrO_3$	29	$InCrO_3$	59
$YMnO_3$	49	$DyCrO_3$	29	$YbGaO_3$	56
$YFeO_3$	51	$ErCrO_3$	29	$GdGaO_3$	56
$LaFeO_3$	29	$LuCrO_3$	29	$CeMnO_3$	66
$YCrO_3$	51	$DyFeO_3$	29	$PrMnO_3$	66
$GdFeO_3$	29	$HoFeO_3$	29	$NdMnO_3$	66
$EuFeO_3$	29	$ErFeO_3$	29	$EuInO_3$	59
$SmFeO_3$	29	$YbFeO_3$	29	$YlnO_3$	59
$NdFeO_3$	29	$LuFeO_3$	29	$SmMnO_3$	66
$PrFeO_3$	29	$LaScO_3$	29	$NdVO_3$	52
$LaCrO_3$	29	$SmScO_3$	29		
A-M_2O_3	ref	A-M_2O_3	ref	A-M_2O_3	ref
Ce_2O_3	27	Nd_2O_3	27	La_2O_3	27
Pr_2O_3	27	$LaSmO_3$	28		
rare earth *P*6_3/*mmc*	ref	rare earth *P*6_3/*mmc*	ref	rare earth *P*6_3/*mmc*	ref
$YAlO_3$	68	$DyAlO_3$	68	$GdInO_3$	60
$EuAlO_3$	68	$HoAlO_3$	68	$DyInO_3$	60
$GdAlO_3$	68	$ErAlO_3$	68	$YMnO_3$	61
$TbAlO_3$	68	$EuInO_3$	60	$YFeO_3$	71
P6_3/*mmc*	ref	*P*6_3/*mmc*	ref	*P*6_3/*mmc*	ref
$InGaO_3$	69	$InFeO_3$	24	$InMnO_3$	23
r-perovskite	ref	r-perovskite	ref	r-perovskite	ref
$LaAlO_3$	48	$PrAlO_3$	48	$NdNiO_3$	73
$LaGaO_3$	52	$NdAlO_3$	48	$SmAlO_3$	52
$CeAlO_3$	29	$LaNiO_3$	47		
P6_3*cm*	ref	*P*6_3*cm*	ref	*P*6_3*cm*	ref
$YMnO_3$	67	$TmMnO_3$	67	$HoMnO_3$	67
$ScMnO_3$	64	$ErMnO_3$	67	$YbMnO_3$	67
$LuMnO_3$	67	$YGaO_3$	45		
bixbyite	ref	bixbyite	ref	bixbyite	ref
$ScFeO_3$	29	$YbScO_3$	29	$LuScO_3$	29
Sc_2O_3	58	$ScInO_3$	29	$LuInO_3$	29
Y_2O_3	58	$HoInO_3$	29	Lu_2O_3	27
Mn_2O_3	58	$ErInO_3$	29	Yb_2O_3	27
In_2O_3	58	$TmInO_3$	29	Ho_2O_3	27
Tl_2O_3	58	$YbInO_3$	29	$GdLuO_3$	28
$YScO_3$	29	$YInO_3$	11	$DyLuO_3$	28
$ErScO_3$	29				
corundum	ref	corundum	ref	corundum	ref
V_2O_3	20	Ga_2O_3	20	Ti_2O_3	20
Cr_2O_3	20	$FeAlO_3$	11	$InTiO_3$	55
Fe_2O_3	20	$AlGaO_3$	11	$CrAlO_3$	25
Rh_2O_3	20	$CrVO_3$	55	$FeCrO_3$	25
Al_2O_3	20	$GaFeO_3$	25		
B-M_2O_3	ref	B-M_2O_3	ref	B-M_2O_3	ref
Eu_2O_3	27	Sm_2O_3	28	$LaHoO_3$	28
Gd_2O_3	27	$LaDyO_3$	28	$NdErO_3$	28
$LaGdO_3$	28				
ilmenite	ref	ilmenite	ref	ilmenite	ref
$CdTiO_3$	57	$CoMnO_3$	57	$FeTiO_3$	57
$CdSnO_3$	57	$NiTiO_3$	57	$MnGeO_3$	57
$NiMnO_3$	57	$MgTiO_3$	57	$MnTiO_3$	57
$MgGeO_3$	57				

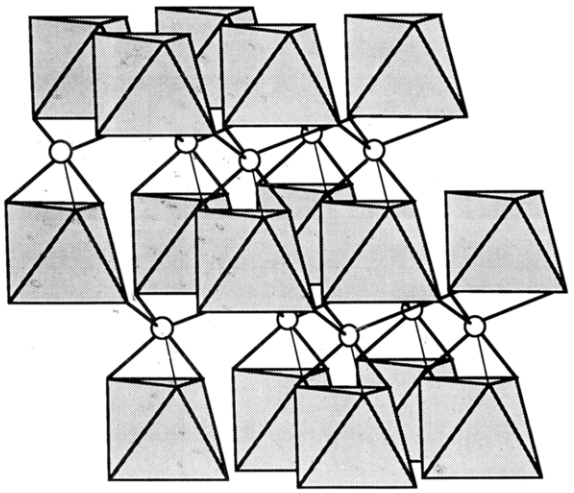

Figure 2. Corundum and the ilmenite structure. The corundum structure if both polyhedra and circles represent the same element or a statistical distribution of different elements; the ilmenite structure if the polyhedra and circles represent different elements in an ordered arrangement.

formation of additional ABO_3 materials with this structure type are presented.

Discussion of ABO_3 structures

Ionic solids can be described using a combination of electrostatic and geometrical arguments. This leads to general approaches for predicting and rationalizing structures based on valence, coordination number, and ionic radii of the cations and anions. Generally, for trivalent ABO_3 structures, there exist two extreme cases: (1) A and B cations of approximately equal size and of a size suitable for coordination within the octahedral interstitial site of a closest-packed oxide framework; (2) an A cation comparable in size to O^{2-} which together with oxygen can form AO_3 closest-packed layers with high coordination numbers in the A site.[20] Oxides of the first group tend to adopt sesquioxide structures, such as corundum (α-Al_2O_3)[20,29] or ilmenite,[38,39] while oxides of the second group form linked BO_6 octahedra and AO_3 closest-packed layers, such as perovskite,[30,31] $BaNiO_3$,[40] or hexagonal $BaTiO_3$ type structures.[41] Uncommon structure types, e.g., $PbReO_3$,[42] the tunnel structure of $KSbO_3$,[43,44] $InMnO_3$,[23] and $LuMnO_3$,[45] often crystallize on or near the border between the sesquioxide structures and the linked BO_6 structures.

The corundum structure, α-Al_2O_3 (Figure 2), is formed by cations having the same oxidation state and/or similar radii and consists of a hexagonal closest-packed oxygen framework in which the trivalent cations are randomly distributed in two thirds of the available octahedral interstices. The regular cation arrangement of the ilmenite structure, on the other hand, is preferred by cations having different oxidation states and/or different radii. According to geometric arguments, the octahedral interstices in close-packed oxygen layers will accommodate ions with radii approximately equal to $(\sqrt{2}-1)r$ or $0.41r$, where r is the radius of O^{2-}, 1.38 Å. This relationship, however, is an approximation, and a certain degree of deviation from the ideal close-packed state may be expected.

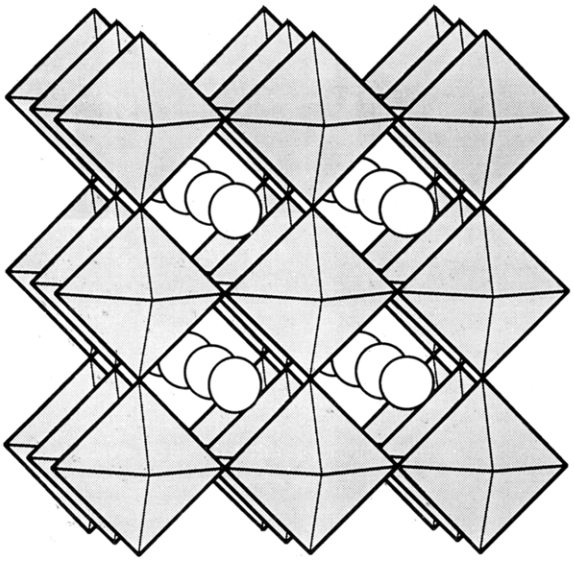

Figure 3. Perovskite structure. The A cations are represented by circles and the B cations are located at the center of the polyhedra; oxygen atoms are located at the apices of the polyhedra.

The ideal perovskite structure (Figure 3) is cubic with the A cation in 12-fold coordination and the B cation in 6-fold coordination. The A-site is located at the body center of the cube, the B site at each of the eight corners, and the oxygen atoms at each of the centers of the 12 edges. Perovskite and distorted perovskite-type structures form for trivalent A and B cations having a range of radii, provided the A cation is large enough to form close-packed layers with O^{2-}, and the B cation is small enough to adopt an octahedral oxygen coordination environment. Under pressure, however, the stability range of the perovskite structure for smaller A cations can be increased. Regardless, as the radius of the A cation decreases, the A and B cations will ultimately adopt a different crystal structure, often the corundum structure, which can better accommodate cations that are both smaller and closer in size to one another.

In the cation size regime bracketed by the lower stability range of the perovskite structure and the upper radius limitations of the corundum structure, the cubic rare-earth structure, C-M_2O_3, or bixbyite,[46] often forms (Figure 4). The bixbyite structure is related to that of fluorite (CaF_2) and may be derived from the fluorite structure by the removal of one-quarter of the anions and subsequent rearrangement. Two types of cation coordination environments are generated, both of which have six instead of eight neighbors at the vertices of a cube; two anions are missing at the ends of a body diagonal and two at the end of a face diagonal, respectively.

To predict which one of the above-mentioned structures will be favored for a given pair of cations, the radius ratio or a more complex radius relationship that includes structure-specific geometric arguments must be calculated. One such relationship is the Goldschmidt tolerance factor:[4]

(40) Takeda, Y.; Kanamaru, F.; Shi Madra, M.; Koizumi, M. *Acta Crystallogr.* **1976**, *B32*, 2464.
(41) Burbank, R.; Evans, H., Jr. *Acta Crystallogr.* **1948**, *1*, 330.
(42) Longo, J. M.; Raccah, R. M.; Goodenough, J. B. *Mater. Res. Bull.* **1969**, *4*, 191.
(43) Hong, H. Y.; Kafalas, J. A.; Goodenough, J. B. *J. Solid State Chem.* **1974**, *9*, 345.
(44) Goodenough, J. B.; Kafalas, J. A. *J. Solid State Chem.* **1973**, *6*, 493.
(45) Geller, S.; Curlander, P. J.; Jefferies, J. B. *Acta Crystallogr.* **1975**, *B31*, 2770.
(46) *Structure Reports*; Hermann, C.; Lohrmann, O.; Philipp, H., Ed.; Verlag: Leipzig, 1928–1932; Vol. 2, p 38.

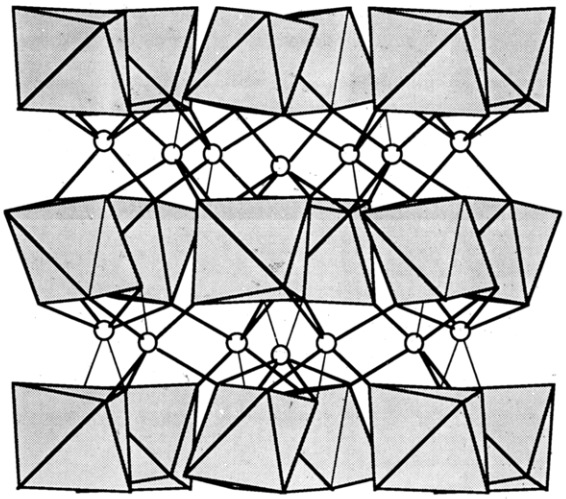

Figure 4. Bixbyite structure. One cation coordination site is represented as a circle and one cation coordination site is located at the center of the polyhedra. Oxygen atoms are located at the apices of the polyhedra.

$$t = \frac{(r_A + r_O)}{\sqrt{2}(r_B + r_O)}$$

The calculation of tolerance factors can be predictive as to which structure type should form. The Goldschmidt tolerance factor was calculated to determine the geometric constraints necessary for the formation of the perovskite structure. However, as previously mentioned, when the perovskite structure does not form, generally sesquioxide structures are stable. For example, for $1 > t > 0.8$, the perovskite structure often forms, while for $0.8 \geq t$ the sesquioxide structures form. The radii used for these calculations, however, are very susceptible to coordination number. Consequently, the addition of pressure may increase the coordination of certain atoms and alter the stability range of a given structure type.

In the absence of applied pressure, combinations of many trivalent first-row transition-metal oxides, including those of iron(III) and manganese(III), and rare-earth oxides form the orthorhombic or rhombohedral form of the perovskite structure as the thermodynamically stable phase.[11,29,47-55] The application of pressure enables smaller A cations, such as scandium and indium, to crystallize in the perovskite structure.[56-59] Low-temperature, kinetic phases also exist, particularly for the rare-earth manganates and the small rare-earth ferrates.[45,50,60-67] In these systems, a hexagonal phase forms below 1000 °C but converts to the perovskite structure at high temperatures and pressures. The rare-earth aluminates form a different but related hexagonal phase[63,68] that also converts to the perovskite structure above 900 °C.

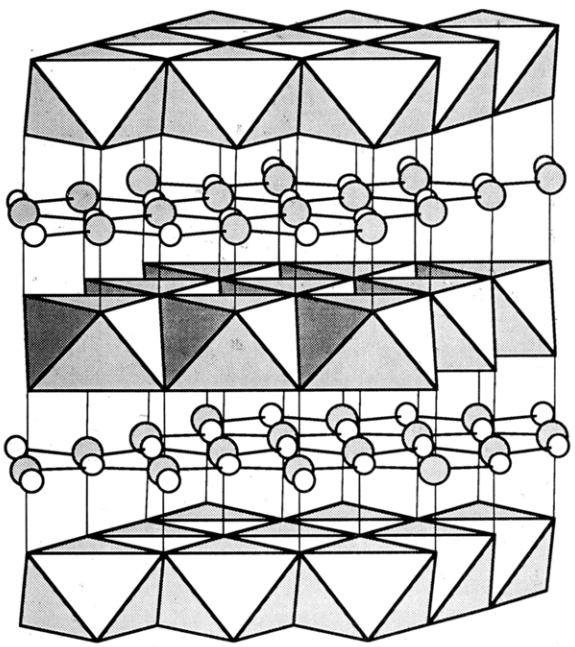

Figure 5. $InMO_3$ structure. Indium atoms are located at the center of the polyhedra; the M atom site, M = Fe, Mn, is represented as a large circle at the center of a trigonal bipyramid of oxygen. Oxygen atoms located within the plane of the M cation are represented as small open circles, while the remainder of the oxygen atoms are located at the apices of the polyhedra.

Unlike the high-temperature thermodynamic phases studied by Roth,[11,29] low-temperature phases containing cations whose radius ratio places them near the bixbyite and ilmenite regions in the trivalent ABO_3 structural phase diagram (Figure 1) have been relatively unstudied. This middle region, where the radii of A and B are too different for the corundum structure to form, or where A is too small to form AO_3 layers, and yet too large to enter interstitial sites in closest-packed oxygen layers, can give rise to many interesting low temperature phases.[24,50,60-69] Due to the many competing interactions that determine the final structure for a given cation pair, kinetic factors can play a crucial role by favoring some of the interactions at the expense of others, thereby favoring structure types that might not form under strictly thermodynamic control.

Discussion of the $InMnO_3$ and $InFeO_3$ Structure: Comparison with the Related $YAlO_3$ Structure

Recently we reported the structure of $InMnO_3$ which consists of alternating layers of octahedrally coordinated indium and trigonal bipyramidally coordinated transition metal atoms[23,24] (Figure 5). The transition metal and indium coordinates are fixed by symmetry and, consequently, have ideal D_{3h} and near ideal octahedral sym-

(47) Wold, A.; Post, B.; Banks, E. *J. Am. Chem. Soc.* **1957**, *79*, 4911.
(48) Geller, S.; Bala, V. B. *Acta Crystallogr.* **1956**, *9*, 1019.
(49) Wood, V. E.; Austin, A. E.; Collings, E. W.; Brog, K. C. *J. Phys. Chem. Solids* **1973**, *34*, 859.
(50) Quezel, S.; Rossat-Mignod, J.; Bertaut, E. F. *Solid State Commun.* **1974**, *14*, 941.
(51) Geller, S.; Wood, E. A. *Acta Crystallogr.* **1956**, *9*, 563.
(52) Geller, S. *Acta Crystallogr.* **1957**, *10*, 243.
(53) Dalziel, J. A. W. *J. Chem. Soc.* **1959**, 1993.
(54) Wood, E. A. *Acta Crystallogr.* **1951**, *4*, 353.
(55) Keith, M. L.; Roy, R. *Am. Mineral.* **1954**, *39*, 1.
(56) Marezio, M.; Remeika, J. P.; Dernier, P. D. *Mater. Res. Bull.* **1966**, *1*, 247.
(57) Reid, A. F.; Ringwood, A. E. *J. Geophys. Res.* **1969**, *74*, 3238.
(58) Reid, A. F.; Ringwood, A. E. *J. Geophys. Res.* **1975**, *80*, 3363.
(59) Shannon, R. D. *Inorg. Chem.* **1967**, *6*, 1474.
(60) Schneider, S. J. *J. Res. NBS* **1961**, *65A*, 429.
(61) Lukaszewicz, K.; Karut-Kalicinska, J. *Ferroelectrics* **1974**, *7*, 81.
(62) Koehler, W. C.; Yakel, H. L.; Wollan, E. O.; Cable, J. W. *Phys. Lett.* **1964**, *9*, 93.
(63) Bertaut, E. F.; Buisson, G.; Durif, A.; Mareschal, J.; Montmory, M. C.; Quezel-Ambrunaz, S. *Bull. Soc. Chim. Fr.* **1965**, 1132.
(64) Komissarova, L. N.; Pokrovskii, B. I.; Shaplygin, I. S. *Neorg. Mater.* **1966**, *2*, 275.
(65) Bertaut, E. F.; Mercier, M.; Pauthenet, R. *J. Phys.* **1964**, *25*, 550.
(66) Pauthenet, R.; Veyret, C. *J. Phys.* **1970**, *31*, 65.
(67) Yakel, H. L.; Koehler, W. C.; Bertaut, E. F.; Forrat, E. F. *Acta Crystallogr.* **1963**, *16*, 957.
(68) Bertaut, E. F.; Mareschal, J. *Compt. Rend.* **1963**, *275*, 867.
(69) Shannon, R. D.; Prewitt, C. T. *J. Inorg. Nucl. Chem* **1968**, *30*, 1389.

metry, respectively. The indium is located in CdI_2-like[20] octahedral interstices between two closest-packed oxygen layers, resulting in edge-shared indium octahedra whose three-fold axis runs parallel to the c direction of the hexagonal unit cell. The 3-fold axis of the trigonal bipyramids also runs parallel to the c direction in a staggered arrangement, such that transition-metal layers repeat with every second layer.

There are unexpected structural differences between $InMnO_3$ and $InFeO_3$ which cannot be attributed to size or geometry arguments alone. According to Shannon's atomic radii tables,[70] the ionic radius of both Mn(III) and Fe(III) in 5-fold coordination is 0.58 Å. Considering that the positions of the transition metal atoms and the indium atoms are fixed in x,y,z and considering that $InMnO_3$ is only slightly larger in the a plane than in $InFeO_3$, the fact that $InFeO_3$ is 0.7 Å taller, 12.1750(1) vs 11.4752(6) Å, in the z direction may be due to electronic differences. This difference most likely results from the electronic configurations of high-spin Mn(III), d^4, and high-spin Fe(III), d^5, and the filling of the d_{z^2} orbital. Since the symmetry of the transition metals is ideal D_{3h}, the energy levels of the 2:2:1 splitting of the d orbitals must adapt to accommodate both d^4 and d^5 ions. Consequently, the difference in c axis lengths between the manganese and iron compounds can be explained by a weakening and elongation of the axial Fe–O bond to effect a lowering in the energy level of the d_{z^2} orbital. This results in an Fe–O(1) distance that is 0.18 Å longer than the corresponding Mn–O(1) distance, as well as an in-plane trigonal Fe–O(2) distance that is shorter than the apical Fe–O(1) distance in $InFeO_3$, while for $InMnO_3$ the opposite is true.

The difference between both $InMnO_3$ and $InFeO_3$, and the related $YAlO_3$[63,68] is even more dramatic. $YAlO_3$ is larger than $InMnO_3$ in the a plane, 3.680(5) vs 3.3985(2) Å; however, the c parameter is dramatically shorter, 10.52(1) vs 11.48 Å. The Al–O bond lengths in $YAlO_3$ are surprisingly similar to the Fe–O bonds found in $InFeO_3$, i.e., short apical bonds and long in-plane bonds, even though the c axis is almost 2 Å shorter, 10.52 vs 12.18 Å. The in-plane trigonal Al–O distances are 2.12(1) Å, while the apical Al–O distances are 1.82(1) Å. The contraction of the c axis in $YAlO_3$ seems to be related to the coordination of the rare-earth atom. Yttrium increases its coordination from 6- to 8-fold coordination because the z axis contraction enables the yttrium to bond with two additional next-nearest neighbor oxygens. In the case of indium, however, this contraction is not necessary, as indium adopts a 6-fold coordination and the oxygen atoms in question are beyond the combined van der Waals radii of indium and oxygen. This contraction is a function of the rare earth atom in the A site, and, consequently, the A cation coordination in $InMnO_3$ is different from that in $YAlO_3$ and $YFeO_3$.[71] The only reported material isostructural with $InMnO_3$ is $InGaO_3$,[69] a high-pressure phase.

Discussion of the $A^{3+}B^{3+}O_3$ Structural Phase Diagram

The Goldschmidt tolerance factor, t, calculated for $InMnO_3$ and $InFeO_3$ is 0.79, at the border of the perovskite, the corundum/ilmenite and the bixbyite structures. Size and ionicity arguments are presented to rationalize the existence of these phases, as well as to predict other ABO_3 materials which may form with this hexagonal structure type. According to the existing structural phase diagram by Roth for trivalent ABO_3 compounds (Figure 1), these unusual hexagonal phases are unexpected. Furthermore, there are other low-temperature hexagonal phases that also cannot be accommodated in the high temperature ABO_3 phase diagram, namely, rare earth manganates and chromates with the related $LuMnO_3$ structure.[45,50,60–67]

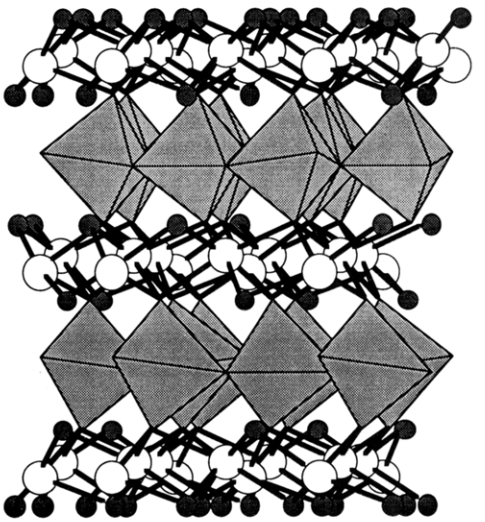

Figure 6. $LuMnO_3$ structure. The rare-earth atoms are seven-coordinate and are represented as white circles. The manganese atoms are in distorted trigonal bipyramidal coordination, represented as polyhedra. Oxygen atoms are represented as shaded circles and are located at the apices of polyhedra.

The $LuMnO_3$ structure, Figure 6, unlike $InMnO_3$ or $InFeO_3$, has a very distorted trigonal bipyramidal coordination site and, consequently, can accommodate Jahn–Teller ions such as Cr(III) d^3, which are not electronically allowed in the ideal D_{3h} coordination site in the $InMnO_3$ structure.

The fact that Mn(III) also exists in this distorted configuration suggests the presence of mixed valency for manganese, a possibility that has been previously suggested.[67,72] Compounds with the $LuMnO_3$ structure convert to either the orthorhombic or rhombohedral distortion of the perovskite structure above 1000 °C, unlike both $InMnO_3$ and $InFeO_3$, which decompose to binary oxides under these conditions. Perhaps In(III) is too small to allow the transformation into the perovskite structure with Mn(III) and Fe(III) at ambient pressure. Perovskite compounds of iron and manganese usually have a tolerance factor of 0.89, while the indium–transition metal oxides have tolerance factors of 0.79. If the radii of indium and iron or manganese were much closer, either the corundum structure or the bixbyite structure could crystallize. As they are, however, the small tolerance factor of indium with most 3+ transition metals will preclude both the corundum and the perovskite structure from forming except under high pressure. At high temperatures and pressures, the stability range of the perovskite structure is increased, allowing some compounds to be stable, e.g., $InRhO_3$,[59] which under pressure takes on the perovskite structure although $t = 0.80$.

(70) Shannon, R. D. *Acta Crystallogr.* **1976**, *A32*, 751–767.
(71) Yamaguchi, O.; Takemura, H.; Yamashita, M. *J. Electrochem. Soc.* **1991**, *138*, 1492.
(72) Gallagher; McCarthy *JCPDS Grant-in-Aid-Report* **1973**.
(73) Vassiliou, J. K.; Hornbostel, M.; Ziebarth, R.; DiSalvo, F. J. *J. Solid State Chem.* **1989**, *81*, 208.
(74) Wold, A.; Post, B.; Banks, E. *J. Am. Chem. Soc.* **1975**, *79*, 6365.
(75) Wold, A.; Arnott, R. J.; Croft, W. *Inorg. Chem.* **1963**, *2*, 972.

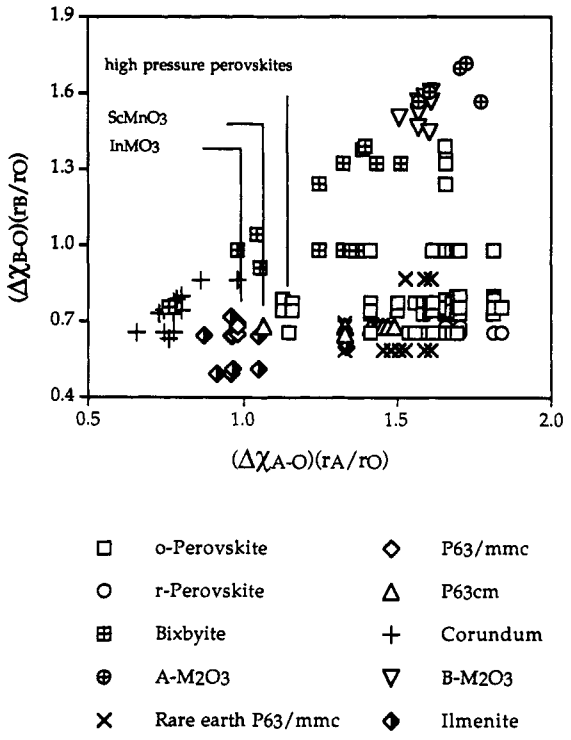

Figure 7. Ionicity graph of the ABO_3 structural phase diagram for common structure types of the compounds listed in Table 1.

Structural Regions in the ABO_3 Phase Diagram

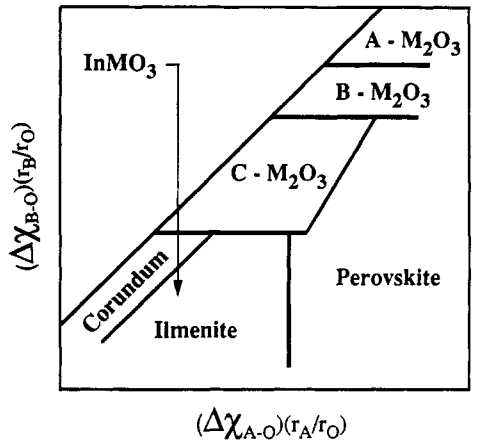

Figure 8. Structural regions within the ABO_3 phase diagram.

A modification of the structural phase diagram used by Roth is presented in Figure 7, and a general structure map is shown in Figure 8. Rather than simply plotting the radius of A vs B, the axes are modified to include the bond ionicities of the A and B cations. As shown by Mooser and Pearson,[8] the bond ionicity can be modeled by the difference in the electronegativity of A and B. Accommodating ABO_3 compounds necessitates the plotting of parameters associated with the character of A–O bonding vs parameters associated with the character of B–O bonding. The approach used by Roth, while quite successful in predicting the most common structure types, is unable to predict the $InMnO_3$-type structures nor able to accommodate materials such as those with the $LuMnO_3$ structure, which convert to the perovskite structure at high temperatures. Using the difference in electronegativity of A–O and B–O and multiplying them by the cation to anion ratio, r_A/r_O and r_B/r_O, respectively, introduces the concept of bond ionicity into Figure 7, and perhaps generalizes this concept for materials with anions other than oxygen, e.g., nitrides, chalcogenides, or halides.

It has been argued for intermetallic systems that it is not possible to accurately differentiate between structure types using less than three dimensional plots.[1] In the case of ABO_3 structures, however, it is possible to use two-dimensional structure–composition diagrams. To include quaternary systems, such as $ABCO_x$, on the other hand, a three-dimensional diagram would undoubtedly achieve better structural separation than an averaged two-dimensional one.

The distribution of structures in Figures 7 and 8 shows the corundum region well separated from the bixbyite region and both apart from the perovskite region. Unlike Figure 1, where $InMnO_3$ and $InFeO_3$ fall too close to the corundum and bixbyite regions to be distinguished based on their radii alone, in Figure 7, the $InMnO_3$ structure type is clearly within the ilmenite region. Thus, by combining the bond ionicities with the cation ratios, we see that an $A^{3+}B^{3+}O_3$ phase, which according to size and ionicity ratios falls into the $A^{2+}B^{4+}O_3$ ilmenite region, requires a new structure type to gain stability. Apparently, in the intermediate size regime where the A cation fits into the bixbyite region and the B cation into the corundum structure, conditions are favorable for the formation of the $InMnO_3$ structure. The $InMnO_3$ structure is separated from the perovskite region by other compounds having unexpected structures, including $ScMnO_3$ and perovskites including $InRhO_3$, which can be synthesized only at pressures high enough to force indium into a coordination higher than six. The perovskite region in the ionicity diagram appears quite complex; however, it should be noted that all of the nonperovskite phases which appear in the perovskite region will convert to the perovskite structure at high temperatures, e.g., $LuMnO_3$ and rare-earth aluminate phases.

It should also be noted that for compounds in which both the A and B cations are rare-earth elements, the ionicity structure map is less useful. (See rare earth regions in Figures 1 and 7.) In this case the use of ionic radii and radius ratio rules alone is more advantageous for structural prediction. This is due to the fact that unlike for both the d-block and the p-block elements, the electronegativity of the f-block elements does not change in a regular fashion as one goes from the left side of the periodic table to the right. Instead, the electronegativities of the rare-earth elements fluctuate across the row. The combination of electronegativity and ionic radius thus negates changes that occur in the ionic radii (the lanthanide contraction) across the row of lanthanides. Consequently, the use of ionicity to predict the structures of compounds containing only f-block elements is not advantageous.

The most useful information is obtained by using the bond ionicity diagram (Figure 7) in conjunction with the ionic radii diagram (Figure 1). The diagram constructed from only ionic radii is quite successful in segregating the major structural types into general areas, particularly for the high-temperature phases. The bond ionicity diagram (Figure 7) complements the ionic radii diagram for features that the ionic radii diagram lacks. Specifically, certain structural areas are more effectively separated in the ionicity diagram, e.g., the corundum region and the ilmenite region. The ionicity diagram also places low-temperature structures and unusual ABO_3 structures closer to their expected locations, e.g., the $(RE)AlO_3$ structures,

high-pressure perovskites, and $ScMnO_3$.

The utility of structure–composition diagrams lies not so much in rationalizing the structures of known compositions, but in predicting the structures of new compositions. For example, based on the diagram shown in Figures 1 and 7, it is possible to predict other phases which may crystallize in the $InMnO_3$ structure. Considering both the geometric and the electronic requirements of the $InMnO_3$ materials, several other compounds may be stable in this structure type according to the diagram shown in Figure 7. For example, $InVO_3$ containing V(III) d^2, which is not a Jahn–Teller ion in D_{3h} symmetry, and $InRhO_3$, containing low-spin Rh(III), are both expected to form the $InMnO_3$ structure type. Also, compounds in which scandium or gallium has replaced indium may crystallize in this structure type, provided that the proper synthetic techniques are employed. The proximity of the $InMnO_3$ structure to the corundum, bixbyite, and perovskite structures emphasizes the delicate nature of the low-temperature synthesis which must be performed in order to favor the $InMnO_3$ structure over other possibilities.

Conclusions

"The proof of the pudding is in the eating." Structure–composition diagrams that correctly predict the structures of new compositions are obviously useful to the synthetic chemist, while those that do not will be quickly discarded. No single approach, so far, can be applied successfully to all classes of solid-state materials, e.g. intermetallics oxides, nitrides, and borides. Nonetheless, structural prediction of solid-state materials using easily obtainable parameters remains an important problem. As new approaches are explored, the goal of the predictable, if not the rational, design of new materials will be more within reach.

Acknowledgment. We thank Professor Jean Rouxel for valuable discussions. This work was supported by the Massachusetts Institute of Technology, Center for Materials Science and Engineering, Grant DMR 9022933.